NASA TECHNICAL NOTE
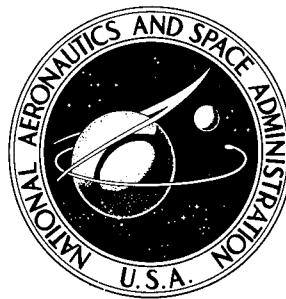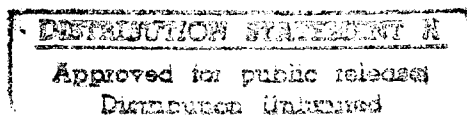
NASA TN D-6463

DTIC QUALITY INSPECTED 2

DESIGNING FOR IMPACT RESISTANCE
WITH UNIDIRECTIONAL FIBER COMPOSITES

by Christos C. Chamis, Morgan P. Hanson,
and Tito T. Serafini

Lewis Research Center
Cleveland, Ohio 44135

19960610 124

1. Report No. NASA TN D-6463	2. Government Accession No.	3. Recipient's Catalog No.
4. Title and Subtitle DESIGNING FOR IMPACT RESISTANCE WITH UNIDIREC- TIONAL FIBER COMPOSITES		5. Report Date August 1971
		6. Performing Organization Code
7. Author(s) Christos C. Chamis, Morgan P. Hanson, and Tito T. Serafini		8. Performing Organization Report No. E-6254
9. Performing Organization Name and Address Lewis Research Center National Aeronautics and Space Administration Cleveland, Ohio 44135		10. Work Unit No. 129-03
		11. Contract or Grant No.
		13. Type of Report and Period Covered Technical Note
12. Sponsoring Agency Name and Address National Aeronautics and Space Administration Washington, D.C. 20546		
		14. Sponsoring Agency Code

15. Supplementary Notes

16. Abstract

Composite micromechanics and macromechanics and the miniature Izod impact test are used to investigate the impact resistance of unidirectional composites. Several composite systems are examined both theoretically and experimentally. The composites are classified theoretically relative to their impact resistance for longitudinal, transverse, and shear modes. Experimental results are reported only for Izod impact with the fibers either parallel or transverse to the cantilever longitudinal axis. Impact resistance design criteria which evolved during this investigation are used to design hybrid composites with improved impact resistance. This is illustrated theoretically and demonstrated experimentally. Approximate design procedures using the impact factor are described. The results show that in-situ fiber and matrix elongation-to-fracture, matrix modulus, fabrication process, fiber and void volume ratios, and microresidual stresses are variables which affect the impact resistance. The ranking of composite impact resistance on the basis of measured and predicted results was in excellent agreement.

17. Key Words (Suggested by Author(s)) Fiber composites; hybrid composites; stress analysis; structural analysis; design; impact; micromechanics; microresidual stress; impact factor; debonding; delamination; Izod impact	18. Distribution Statement Unclassified - unlimited		
19. Security Classif. (of this report) Unclassified	20. Security Classif. (of this page) Unclassified	21. No. of Pages 42	22. Price* $3.00

DESIGNING FOR IMPACT RESISTANCE WITH UNIDIRECTIONAL

FIBER COMPOSITES

by Christos C. Chamis, Morgan P. Hanson, and Tito T. Serafini

Lewis Research Center

SUMMARY

Composite micromechanics, macromechanics, and the miniature Izod impact test are used to investigate the impact resistance of unidirectional composites. Several composite systems are examined both theoretically and experimentally. The composites are classified theoretically relative to their impact resistance for longitudinal, transverse, and shear modes. Experimental results are reported only for Izod impact with the fibers either parallel or transverse to the cantilever longitudinal axis. Impact resistance design criteria which evolved during this investigation are used to design hybrid composites with improved impact resistance. This is illustrated theoretically and demonstrated experimentally. Approximate design procedures using the impact factor are described.

The effect of microresidual stress on the longitudinal impact resistance is examined theoretically for composites with fiber-to-matrix modulus and/or stress ratio of approximately four.

Predicted and measured results are compared on a rank or order basis. Measured results consist of those obtained in the experimental portion of this investigation and those available in the literature. Scanning electron microscope photomicrographs of specimen fracture surfaces are also included. Experimental results are presented to show the variation of the transverse impact resistance as a function of composite intralaminar-shear-strength. Photographs of the various impacted test specimens are presented to illustrate the types of failure.

The results show that the in-situ fiber elongation-to-fracture controls longitudinal impact. Debonding and delamination are controlled by matrix modulus and in-situ matrix elongation-to-fracture. Microresidual stresses are detrimental in fiber/metal matrix composites. The ranking of predicted and measured impact resistance is in excellent agreement for several composites which had been evaluated by various methods.

The experimental results indicate that impact can result in three main types of composite fracture modes. These are cleavage, cleavage with fiber pullout, and delamination. Combinations of these modes also take place. The impact resistance of one hybrid composite system investigated was greater than either of the constituent composites.

INTRODUCTION

An important design aspect of fiber composite structural components is their impact resistance. Some basic work on impact resistance and on other closely related properties of these materials has been reported in the literature. See, for example, references 1 to 5. However, the understanding of impact resistance of fiber composites has not advanced to the point where components can be designed for impact using conventional design procedures.

To obtain an insight into the impact resistance of structural components made from fiber composites, we begin by examining their physical make-up. The components considered herein are made by laminating several plies; the ply is itself a unidirectional composite. A better understanding of component impact resistance can then be obtained by investigating the impact resistance of individual plies, multilayer unidirectional composites, the interply matrix layers, and the constituent material properties and fabrication processing variables. This report deals with such an investigation. The investigation is limited to gross-type impact (sufficiently long impact contact times so that the entire component resists the impacting force) and to unidirectional composites which exhibit a linear static stress-strain relation to fracture.

The objectives of the investigation are to obtain a better understanding of impact resistance through elementary theoretical considerations and simple experiments. The experiments are of a qualitative nature and serve as a means to rank the composites. The following factors are examined: interpretation of impact resistance in terms of the energy under the static stress-strain diagram; relation of this energy to constituent material properties and fabrication processing variables; identification of prevalent failure modes; identification of constituent material properties which have a strong influence on impact resistance; construction of design criteria for improving impact resistance; and classification of several available fiber composites on an impact resistance scale.

The theoretical expressions for predicting impact resistance are covered in the section THEORETICAL INVESTIGATION. Here, impact resistance associated with single or combined fracture modes is presented and discussed. Design concepts using hybrid composites and the impact factor are also covered. The detailed derivations are given in the appendix. The experimental investigation is described in the section EXPERIMENTAL INVESTIGATION. In this section, the constituent materials, fabrication process, test specimens, and test methods are described. The experimental results are also discussed in this section. Both theoretical and experimental results are presented in tabular and graphical forms and can serve as an aid in design.

SYMBOLS

A	cross-sectional area
A_D	delaminated area
a	constant defined in eq. (5)
B	constant defined in eq. (5)
b	width
C_1	correlation constant in eq. (8)
d_f	fiber diameter
E	modulus
G	shear modulus
g	gravitational constant
H	height weight dropped
h	member depth
IED	impact energy density
IF	impact factor
K	spring constant
K_{fD}	volume ratio of pullout fibers
K_{Ic}	fracture toughness opening mode
K_{IIc}	fracture toughness shear mode
k_f	fiber volume ratio
k_v	void ratio
L_c	member length over which uniform stress exists
l	length
l_{cr}	fiber debonded length
l_D	delaminated length
N_{fD}	number of pullout fibers
N_{LD}	number of delaminated layers
S	unidirectional composite (ply) strength
S^*	modified S, eq. (17) and (A56)

3

S_{fT}	fiber strength
$S_{\ell\,llc}^{S}$	longitudinal compressive strength
T	temperature
ΔT	temperature difference between composite processing and use temperatures
U	energy, strain energy
V	volume
v	impacting weight velocity
W	impacting weight
x, y, z	structural axes coordinate system
1, 2, 3	material axes coordinate system
α	thermal coefficient of expansion
β	correlation coefficients
β_V	void strain magnification on in-situ matrix
ϵ	strain
ϵ^{*}	composite limit fracture strain
φ_{μ}	matrix strain-magnification-factor
σ	stress
τ	shear strength for interface bond

Subscripts:

C	compression
c	core
cr	critical
D	debonding, delamination
FPO	fiber pullout
f	fiber property
i	summation index
L	longitudinal
ℓ	unidirectional composite (ply) property
m	matrix property
mp	matrix limiting property

4

R   residual stress

S   shear

s   shell

T   tension

x, y, z   directions coinciding with structural axes

1, 2, 3   directions coinciding with material axes

Superscripts:

a   averaged properties

c   core composite

s   shell composite

THEORETICAL INVESTIGATION

In general advanced unidirectional fiber composites exhibit linear stress-strain behavior (fig. 1). Linear stress-strain relations are also retained at high rates of load-
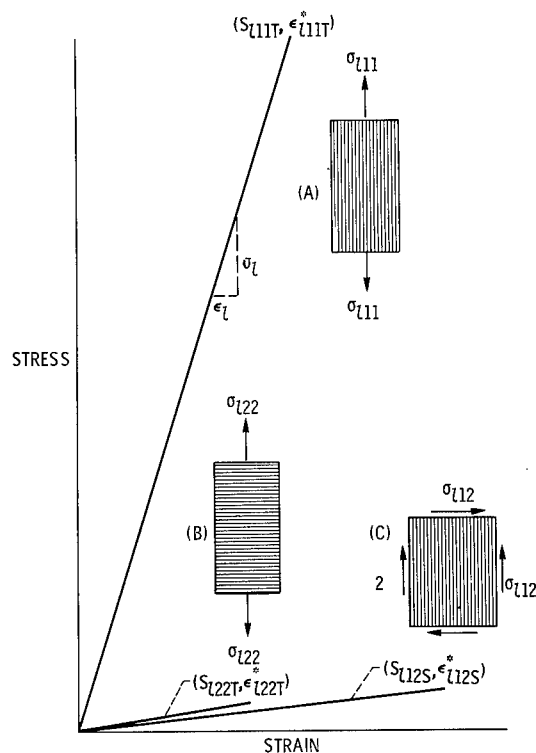

Figure 1. – Typical stress-strain curves of unidirectional fiber composite material subjected to high rate of loading.
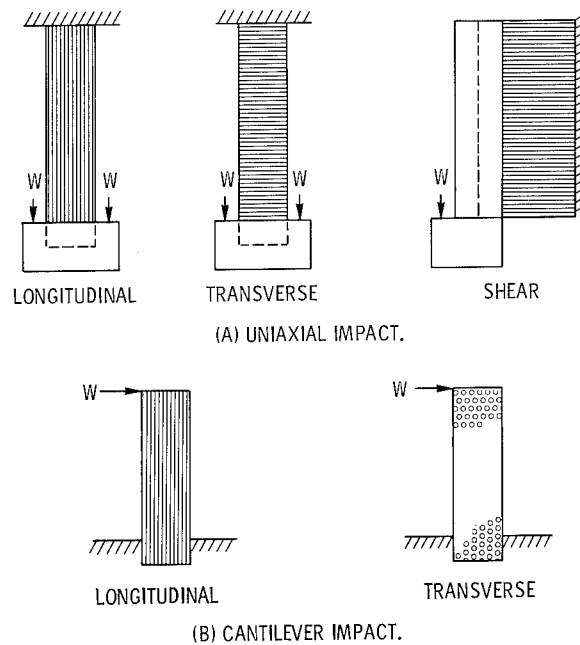
Figure 2. - Composite geometry and impact loadings.

ings (ref. 6). These linear stress-strain relations and composite micromechanics (refs. 7 and 8) form the basis of the theoretical development for computing the impact resistance.

The impact loadings, which are considered here, are illustrated in figure 2. As can be seen in this figure, the impact loadings are either along the material axis of the composite (longitudinal, transverse, or shear) or at the free end of a cantilever.

Longitudinal Impact Resistance

Longitudinal impact loading can result in either of two modes of fracture; these are (1) cleavage - the fracture surface consists of fractured fibers and matrix which lie approximately in the same plane and (2) cleavage with fiber pullout - the fracture surface consists of fractured fibers in combination with debonding and fiber pullout. In the latter case not all of the fracture surfaces of the fibers lie on the same plane. Both of these fracture modes are extensively discussed in references 3, 4, and 9.

Impact-Induced Cleavage Fracture

The equation describing cleavage failure due to impact is obtained by determining the strain energy density. It is shown experimentally in reference 10 that the strain

6

energy density correlates with Izod impact. For longitudinal impact (fig. 1(a)), this is simply

$$U = \frac{1}{2} \epsilon^*_{\ell\,11T} S_{\ell\,11T} V \tag{1}$$

or

$$U = \left(\frac{S^2_{\ell\,11T}}{2E_{\ell\,11}} \right) V \tag{2}$$

where U is the strain energy, ϵ^* is the fracture strain, S is the fracture strength, V is the volume, and E is the modulus. The subscript group $\ell 11T$ is defined as follows: ℓ refers to unidirectional properties, 11 identify outward normal to the plane and stress directions in that order, and T identifies the sense of the stress. By using composite micromechanics (ref. 8) two equations can be derived for $S_{\ell\,11T}$ depending on whether the fibers or the matrix offer the primary resistance to fracture. The derivations are given in the appendix. Only the final equations are given here. The impact energy density (IED) equals the strain energy divided by the volume. The IED of composites with an E_f/E_m ratio greater than 20 is approximated by

$$IED = \frac{(1 - k_v) k_f \beta^2_{fT} S^2_{fT}}{2E_f} \tag{3}$$

with an approximation error of less than 5 percent. The undefined variables in equation (3) are as follows: k_v and k_f denote void and fiber volume ratios, respectively; β_{fT} represents the in-situ fiber strength efficiency which reflects the fabrication process. The subscript f refers to fiber property. The important points to be noted in equation (3) are the quadratic dependence of the strain energy density on the fiber strength S^2_{fT} and the fabrication process variable β^2_{fT}. For a high impact resistance composite, equation (3) imposes the following requirements: a high strength low modulus fiber, approximately 100 percent fiber properties translation efficiency, high fiber volume ratio, and low void volume ratio. Three additional points to be noted here are the following:

(1) The dependence of the strain energy density and therefore impact resistance on S_{fT}/E_f and k_f has been clearly demonstrated in references 11 and 12.

(2) The contribution of $(1 - k_f)\beta^2_{fT}$ is contradictory to the results predicted by the
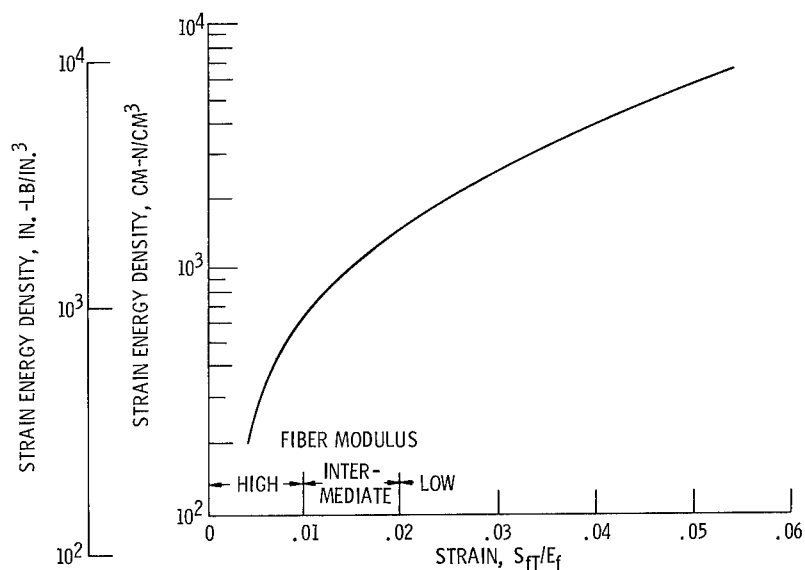
7

Figure 3. – Potential impact resistance of fiber composite materials from table I.

TABLE I. – LONGITUDINAL IMPACT RESISTANCE OF VARIOUS

FIBER/RESIN MATRIX COMPOSITES

[Fiber volume ratio k_f = 0.5; void ratio k_v = 0; in-situ fiber
strength efficiency β_{fT} = 1.0.]

Fiber	Density		Fiber modulus		Fiber strength		Predicted longitudinal impact energy density		
	g/cm^3	$lb/in.^3$	N/cm^2	psi	N/cm^2	ksi	$cm-N/cm^3$	$in.-lb/in.^3$	Rank
Boron	2.62	0.095	414×10^5	60×10^6	3.18×10^5	460	608	880	7
E-glass	2.49	.090	69	10	2.58	360	2240	3250	3
S-glass	2.49	.090	86	12.4	4.62	670	6250	9050	1
Modmor-I	1.99	.072	414	60	1.73	250	179	260	10
Modmor-II	1.74	.063	262	38	2.52	350	656	950	6
Thornel-400	1.71	.062	207	30	2.90	420	1020	1470	5
Thornel-50	1.63	.059	345	50	1.66	240	200	290	9
Thornel-75	1.85	.067	473	75	2.62	380	324	470	8
PRD-49	1.38	.050	173	25	2.76	400	1040	1600	4
UARL-344 glass	3.60	.130	128	18.6	4.83	700	4860	7050	2

8

debonding and fiber pullout mechanism. See section Longitudinal Impact with Cleavage and Fiber Pullout and also references 3 and 4.

(3) Equation (3) is a simple and convenient means to rank fiber composites for longitudinal impact resistance.

A graphical representation of equation (3) for various available composites is shown in figure 3, where the strain energy density is plotted as a function of S_{fT}/E_f (ratio of fiber strength to fiber modulus) which equals in-situ fiber elongation-to-fracture. These same composites have been ranked according to equation (3) in table I. Note that in table I three relatively new fibers have been listed; they are Thornel-400, a high modulus organic fiber (PRD-49), and UARL-344 glass (ref. 13).

Rank comparisons of results reported in the literature with those predicted by equation (3) are shown in table II for notched Charpy impact, in table III for fracture

TABLE II. - COMPARISON OF PREDICTED RESULTS WITH NOTCHED CHARPY IMPACT DATA (REF. 13)

WITH FIBERS PARALLEL TO LONGITUDINAL AXIS OF BEAM

Composite	Fiber volume ratio	Fiber modulus		Fiber strength		Impact energy					
		N/cm^2	psi	N/cm^2	ksi	Measured (ref. 13)			Predicted[a]		
						cm-N	ft-lb	Rank	cm-N/cm	in.-lb/in.	Rank
Thornel-50/epoxy	0.55	345×10^5	50×10^6	1.66×10^5	240	544	4	4	218	315	4
Boron/epoxy	.55	404	58.5	3.18	460	1356	10	3	687	995	3
UARL-344 glass/epoxy	.633	128	18.6	4.83	700	4080	30	2	5760	8 350	2
S-glass/epoxy	.65	85.5	12.4	4.62	670	7340	54	1	8160	11 800	1

[a]Void ratio $k_v = 0$; in-situ fiber strength efficiency $\beta_{fT} = 1.0$.

TABLE III. - COMPARISON OF IMPACT ENERGY DENSITY WITH MEASURED

FRACTURE TOUGHNESS FOR GLASS-FABRIC COMPOSITES

Specimen[a]	Fiber volume ratio[a]	Measured fracture toughness, K_{Ic}[b]			Predicted impact energy density[c]		
		N/cm^2-$cm^{1/2}$ [a]	ksi-in.$^{1/2}$ [a]	Rank	cm-N/cm^3	in.-lb/in.^{3}	Rank
1 - 18	0.545	27.2 to 28.8	24.8 to 26.2	3	1700	2460	3
2 - 18	.476	22.4 to 25.0	20.4 to 22.7	4	1460	2120	4
3 - 18	.589	40.8 to 41.8	37.2 to 38.1	2	1830	2650	2
4 - 18	.676	43.1 to 46.8	39.2 to 41.7	1	2110	3050	1
5 - 18	.294	17.4 to 20.6	15.8 to 18.7	5	912	1320	5
6 - 18	.225	16.4 to 18.0	14.9 to 16.4	6	701	1015	6

[a]Results from table 6 (ref. 11).

[b]Results were obtained from beam splitting tests.

[c]Fiber strength $S_{fT} = 207$ N/cm^2 (300 ksi); fiber modulus $E_f = 6.9\times10^6$ N/cm^2 (10×10^6 psi); void ratio $k_v = 0$; and in-situ fiber strength efficiency $\beta_{fT} = 1.0$.

TABLE IV. - COMPARISON OF IMPACT ENERGY DENSITY WITH MEASURED DATA OF GRAPHITE

FIBER/EPOXY COMPOSITES AT CRYOGENIC TEMPERATURES

[Temperature, T = 20.3° R (-423° F), ref. 19.]

Matrix type (measured)[a]			Fiber volume ratio	Fiber modulus[b]		Fiber strength[b]		Composite fracture energy					
								Measured[a]			Predicted impact energy density		
$cm\text{-}N/cm^2$	$in.\text{-}lb/in.^2$	Rank		N/cm^2	psi	N/cm^2	ksi	$cm\text{-}N/cm^2$	$in.\text{-}lb/in.^2$	Rank	$cm\text{-}N/cm^3$	$in.\text{-}lb/in.^3$	Rank
7.3	10.6	3	0.38	324×10^5	47×10^6	1.59×10^5	230	46	67	4	148	214	4
7.1	10.4	4	.39	338	49	1.64	238	29	42	5	155	225	3
2.9	4.2	6	.40	345	50	2.54	368	152	220	1	372	540	1
8.2	11.9	2	.40	297	43	2.68	289	64	93	2	279	390	2
8.5	12.3	1	.42	332	48	1.50	218	58	84	3	144	208	5
3.4	5.0	5	.41	311	45	.99	143	23	33	6	64	93	6

[a]Measured by beam splitting method (ref. 20).

[b]Reported in ref. 20.

toughness, and in table IV for energy-absorbed-to-failure at cryogenic temperatures. As can be seen in these tables, the ranking comparisons are in excellent agreement.

Effects of Microresidual Stresses on Impact Resistance

The contribution of the matrix to impact resistance is not negligible in composites having a strong and stiff matrix and a good interface bond. For these types of composites, usually $E_f/E_m < 10$, which is typical for fiber/metal matrix composites.

The governing equation for the impact energy density for this case is given by

$$IED = aE_{l\,11}\left(S_{mT} - B\,\frac{k_f}{E_{l\,11}}\right)^2 \tag{4}$$

where

$$\left.\begin{array}{l} a = \dfrac{1}{2E_m^2} \\[2ex] B = \Delta T(\alpha_f - \alpha_m)E_f E_m \end{array}\right\} \tag{5}$$

The subscripts l, f, and m denote ply, fiber, and matrix properties, respectively; α is the thermal coefficient of expansion; and ΔT is the difference between the composite processing and use temperatures.
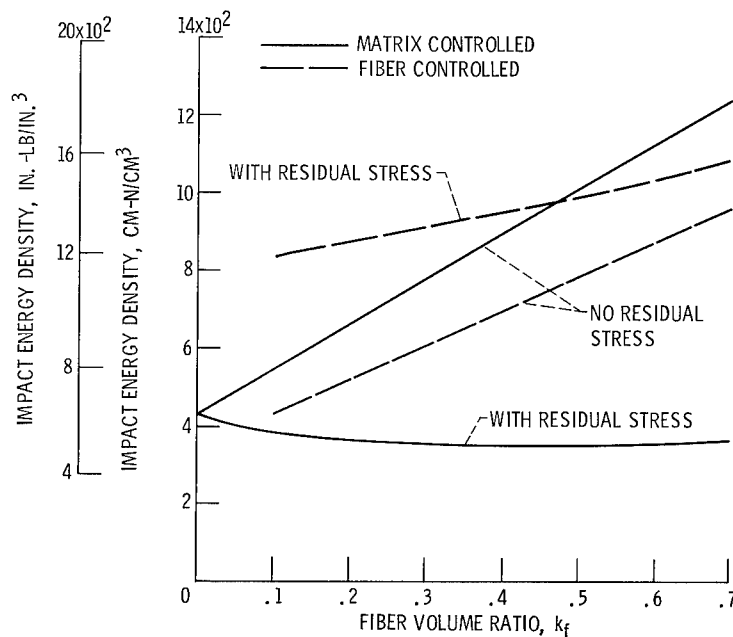
10

Figure 4. - Theoretical longitudinal impact resistance of boron-silicon carbide/titanium unidirectional composite. Processing temperature, 832° C (1500° F).

One very important point to be noted in equations (4) and (5) is that the strain energy density depends significantly on the microresidual stress. The microresidual stress is represented by the parameter B in equation (4). This dependence has not been reported previously in the literature. It is suspected that the presence of microresidual stress in the matrix produced some of the trends reported in references 3 and 14. However, the authors of these references did not attribute the decrease in fracture energy to this phenomenon.

The dependence of the strain energy density and therefore the impact resistance on the microresidual stress is illustrated in figure 4 for a boron-silicon carbide coated/titanium system. Two sets of curves are plotted in this figure. One set is for matrix-controlled failure with and without residual stress. The other set is for fiber-controlled failure with and without residual stress. This second set was obtained from equations (4) and (5) by interchanging the subscripts f and m (see appendix).

The important point to be noted in figure 4 is that impact resistance, or fracture toughness, is very sensitive to the presence of microresidual stresses. Therefore, interpretation of experimental results from composites with $E_f/E_m < 10$ must take the microresidual stress into account.

Longitudinal impact loadings resulting in partial cleavage failure with debonding and fiber pullout is a combined fracture mode. Description of this type of mode will follow the description of the single modes.

11

Transverse Impact Resistance

Transverse impact loadings of unidirectional composites (fig. 2(a)) result in brittle fractures. The amount of energy absorbed to fracture during transverse impact is referred to as the transverse impact resistance. The strain energy divided by the volume of the material is referred to as the IED. This IED as measured under the transverse stress-strain curve is shown in figure 1(b). The governing equation is derived from the stress-strain diagram in figure 1(b) and the micromechanics relations of reference 8. The detailed derivations are presented in the appendix. The resulting equation for the transverse IED is given by

$$ \text{IED} = \frac{1}{2} \left(\beta_{22T} \frac{\epsilon_{mpT}}{\beta_v \varphi_{\mu 22}} \right)^2 E_{l22} \tag{6} $$

The variables in equation (6) are the following: β_{22T} is the correlation coefficient reflecting the fabrication process; ϵ_{mpT} is the maximum transverse strain that the in-situ matrix will experience when the composite is loaded in the transverse direction; β_v is the void magnification of the transverse matrix strain; $\varphi_{\mu 22}$ is the matrix transverse-strain-magnification factor which is a complex function of constituent moduli and fiber content; and E_{l22} is the transverse composite modulus.

There are several important points to be observed in equation (6); they are the following:

(1) The transverse impact resistance is a complex function of the fabrication process, material properties, and composite properties.

(2) The degree of bond at the interface is reflected by β_{22T}; the poorer the interface bond, the smaller the value for this coefficient.

(3) Increases in either void or fiber content or both have inverse square effects on the transverse impact resistance. These effects result in more brittle composite behavior.

(4) The impact resistance increases linearly with the ply transverse modulus.

(5) The impact resistance increases as the square of the in-situ matrix-fracture-strain.

It is important to note that the in-situ matrix-fracture-strain is not the failure strain of the bulk matrix material. For nonmetallic matrixes the former is a small fraction of the latter (ref. 8). The difference between in-situ and bulk matrix-fracture-strain is not widely recognized. As a result, efforts to correlate theory with experiment and to develop matrix materials which would result in improved composite proper-

ties have usually failed. However, both of these disparities can be remedied with suitable micromechanics models and appropriate experiments (results of current unpublished research by the authors).

The graphical representation of equation (6) for typical fiber composites is shown in figure 5. In this figure the transverse IED has been plotted as a function of fiber volume ratio. Three important points to be noted in figure 5 are the following:

(1) The impact resistance of graphite fiber/epoxy composites is insensitive to fiber volume ratio.

(2) However, boron and glass fiber/epoxy composites become quite brittle at high fiber volume ratios (>0.65).

(3) All fiber/nonmetallic composites have approximately the same impact resistance at about 0.50 fiber volume ratio.

The variation of the transverse IED as a function of matrix modulus, is shown in table V for a Modmor-I/epoxy composite. As can be seen in this table, the IED increases very rapidly with increasing matrix modulus. The two reasons for this rapid increase are (1) the matrix-strain-magnification factor $\varphi_{\mu 22}$ decreases rapidly while the composite transverse modulus $E_{\ell 22}$ increases (table V) and (2) the fiber is anisotropic; that is, the transverse fiber modulus is about 0.69×10^6 to 1.3×10^6 newtons per square centimeter (1×10^6 to 2×10^6 psi).
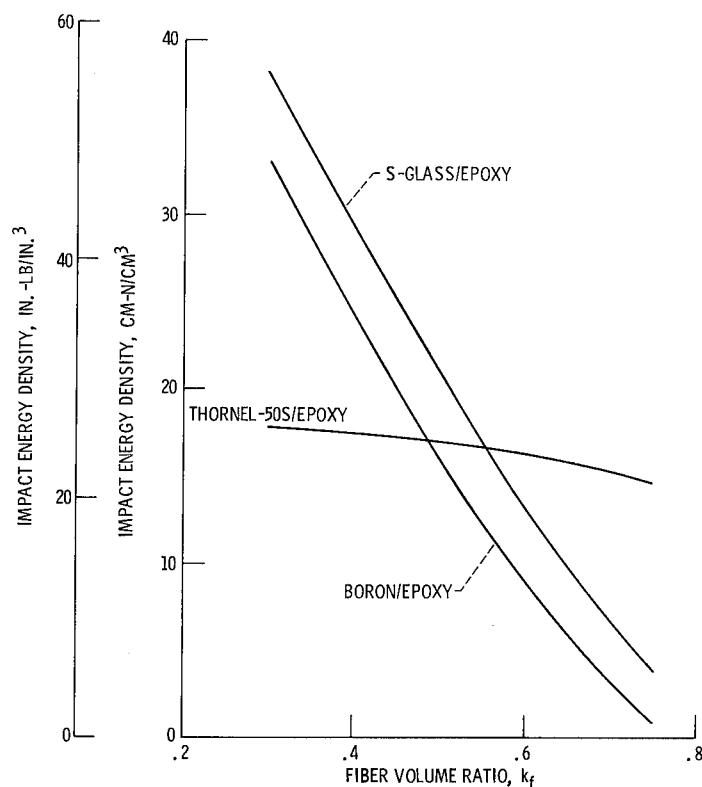

Figure 5. – Theoretical transverse impact resistance of unidirectional composites.

TABLE V. - EFFECTS OF MATRIX MODULUS ON TRANSVERSE AN SHEAR IMPACT ENERGY DENSITY

[Modmor-I/epoxy composite; fiber volume ratio $k_f = 0.5$; void ratio $k_v = 0.$]

Matrix modulus		Strain magnification factors[a]		Unidirectional composite moduli[a]				Predicted impact energy density			
				Transverse		Shear		Transverse		Shear	
N/cm^2	psi	Transverse	Shear	N/cm^2	psi	N/cm^2	psi	$cm-N/cm^3$	$in.-lb/in.^3$	$cm-N/cm^3$	$in.-lb/in.^3$
0.69×10^5	0.1×10^6	3.26	4.37	1.86×10^5	0.27×10^6	0.97×10^5	0.14×10^6	0.93	1.34	4.3	6.2
2.07	.3	1.96	3.54	4.35	.63	2.56	.37	5.67	8.20	17.0	24.6
3.45	.5	1.42	2.97	5.86	.85	3.80	.55	14.6	21.10	36.6	53.1
4.82	.7	1.12	2.56	6.89	1.00	5.18	.75	27.5	39.8	61.9	89.6
6.89	1.0	1.00	2.12	7.95	1.15	6.14	.89	39.7	57.5	115	166
10.03	1.5	1.00	1.65	9.05	1.31	7.66	1.11	45.2	65.5	237	343

[a]Generated with computer code of ref. 18.

Shear Impact Resistance

Shear impact loadings of unidirectional composite (fig. 2(a)) result in relatively brittle fracture. The amount of energy absorbed to fracture during shear impact is called herein shear impact resistance. The corresponding IED as measured under the shear stress-strain curve is shown in figure 1(c). The detailed derivations of the governing equation are described in the appendix. The resulting equation for shear is given by

$$IED = \frac{1}{2}\left(\frac{\beta_{12S}\epsilon_{mpS}}{\beta_v \varphi_{\mu 12}}\right)^2 G_{l\,12} \tag{7}$$

Note the similarity of equations (7) and (6). Corresponding terms have analogous meanings, namely: β_{12S} is the correlation factor; ϵ_{mpS} is the in-situ matrix shear-fracture-strain; β_v is the void contribution to the matrix shear strain; $\varphi_{\mu 12}$ is the matrix shear-strain-magnification factor; and $G_{l\,12}$ is the composite shear modulus in the plane containing the fibers.

The important points noted in discussing equation (6) apply to corresponding terms in equation (7) as well. One additional point to be noted is that equation (7) describes also intralaminar shear delamination which will be described subsequently.

The graphical representation for typical fiber composites is shown in figure 6. In this figure the IED for shear is plotted as a function of the fiber volume ratio. The important points in figure 6 are the following:

(1) Boron/epoxy composites are superior in shear impact as compared with other fiber/epoxy composites when the fiber volume ratio is less than about 0.6.
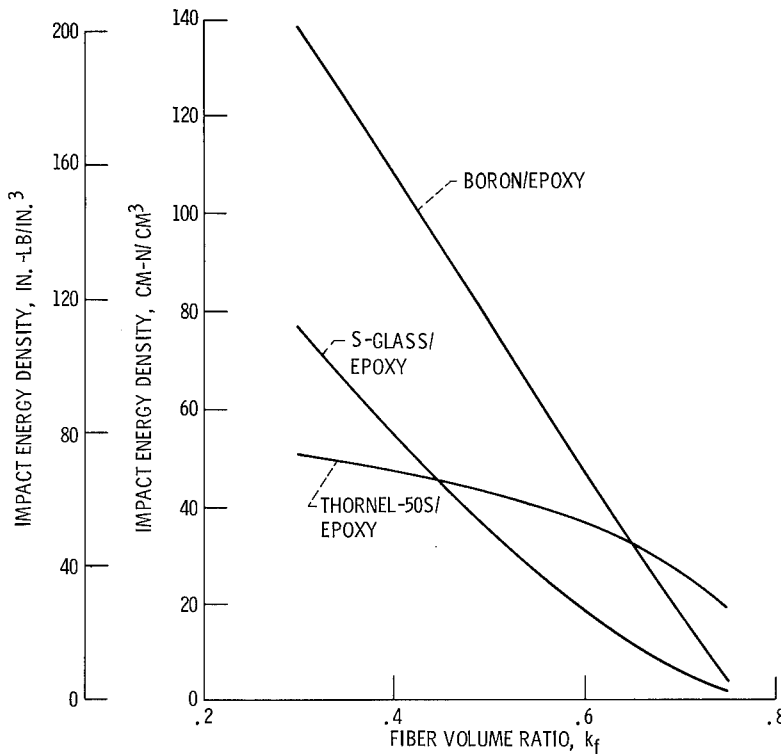
14

Figure 6. - Theoretical shear impact resistance of unidirectional composites.

(2) The shear impact resistance of isotropic boron and S-glass fiber/epoxy composites is very sensitive to fiber volume ratio.

The variation of the shear IED as a function of matrix modulus for a graphite Modmor-I fiber/epoxy composite is shown in table V. As can be seen in this table, the shear IED increases very rapidly with increasing matrix modulus. The reason for this very rapid increase is the variation of the matrix shear-strain-magnification factor and the composite shear modulus (eq. (7) and table V) with increasing matrix modulus. It should be noted that the shear IED increases more rapidly than the transverse IED as can be seen by comparing corresponding columns in table V.

It is interesting to compare equation (7) with equation (17) (from ref. 15) which was derived from fracture mechanics considerations. Equation (17) from reference 15 is repeated here using the notation of this report for convenience

$$K_{\text{IIc}} = C_1 S_{l\,12S} \sqrt[6]{k_v}$$

where K_{IIc} is the critical stress intensity factor (fracture toughness) in the shear mode, C_1 is a correlation coefficient, $S_{l\,12S}$ is the intralaminar (horizontal) shear strength, and k_v is the void volume ratio. By using the micromechanics definition for $S_{l\,12S}$, equation (17) from reference 15 can be expressed as

15

$$K_{IIc} = C_1 \left(\frac{\beta_{12S} \epsilon_{mpS}}{\beta_v{}^{\varphi}{}_{\mu 12}} \right) G_{l\,12} \sqrt[6]{k_v} \qquad (8)$$

Note that the fracture toughness in the shear mode K_{IIc} depends linearly on the in-situ matrix shear-fracture strain ϵ_{mpS} and the composite shear modulus. It is inversely proportional to the matrix shear-strain-magnification factor. The parameter $G_{l\,12}/\varphi_{\mu 12}$ is a nonlinear increasing function of the matrix modulus (table V). The matrix modulus then is a more important parameter in increasing K_{IIc} than the bulk matrix elongation-to-fracture. This observation is not widely recognized in the fiber composite research community. Note also that the shear impact resistance is more sensitive to the parameter $\epsilon_{mpS}/\varphi_{\mu 12}$ than is the fracture toughness. The former depends quadratically on this parameter, while the latter only linearly.

Longitudinal Impact Resistance from Fiber Pullout

Fiber composite fractured surfaces usually exhibit some debonding and fiber pullout. This fracture mechanism has been investigated extensively (refs. 1 to 4).

The following two assumptions are made to derive the governing equation: (1) the energy absorbed during impact is expanded in pulling out the fibers and (2) the interface bond strength is approximated by the intralaminar shear strength. Assumption (2) was first introduced in reference 2. The detailed derivations leading to the governing equation are given in the appendix. The result for the impact energy density from fiber pullout is given by

$$IED = \frac{1}{8} (1 - k_v) \left(\frac{\beta_v{}^{\varphi}{}_{\mu 12}}{\beta_{12S} \epsilon_{mpS}} \right) \frac{S_{fT}^2}{G_{l\,12}} \qquad (9)$$

The symbols in equation (9) have been defined previously. Equation (9) describes IED due to fiber pullout as a complex function depending on fabrication process, fiber and void contents, constituent strength properties, and composite shear modulus. The variation of IED as a function of constituent elastic properties is not easily seen in equation (9) because the parameter $\varphi_{\mu 12}/G_{l\,12}$ depends on fiber and void contents, and on the constituent properties in a complex way. This parameter is defined herein as the "debonding parameter" because it is an indication of the local interface shear bond. Its dependence on matrix modulus and fiber volume ratio is shown in figure 7 for Modmor-I fiber/epoxy composites.
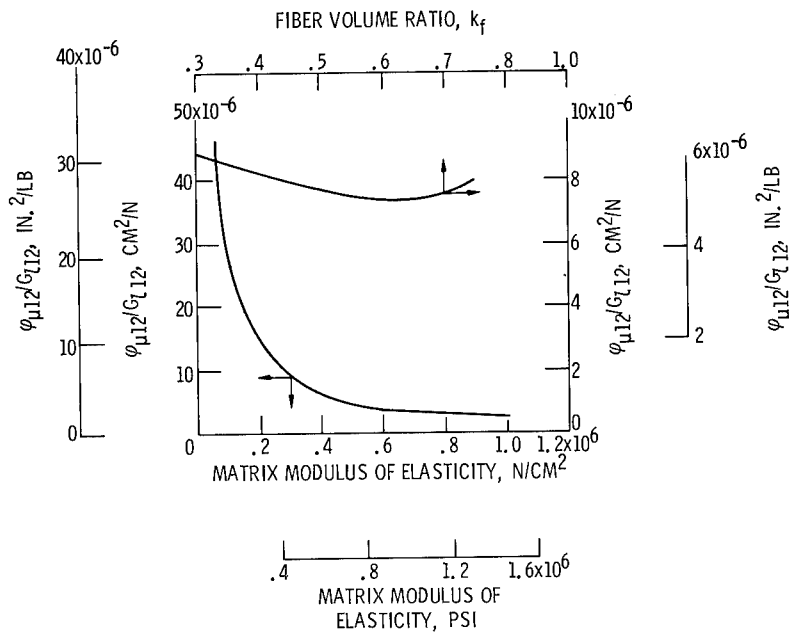
Figure 7. - Debonding parameter for Modmor-I/epoxy composite with zero voids.

The important points to be noted from equations (9) and (A9) in conjunction with figure 7 are the following:

(1) Local bonding is enhanced with increasing fiber volume ratios (up to about 0.65) or increasing matrix modulus.

(2) IED due to debonding can be increased by any or all combinations of the following: poor interface bond, low in-situ matrix elongation-to-failure, large G_{f12}/G_{m12} ratio, and constituents selection which results in low composite shear modulus $G_{\ell 12}$.

It is important to note that the parameters which enhance IED from debonding and fiber pullout are quite detrimental to composite structural integrity with respect to static strength and stiffness.

Impact Resistance Due to Delamination

Delamination in the context used here refers to the delamination due to shear of interply layers in multilayered composites. The energy expanded is referred to herein as the "impact resistance due to delamination."

The governing equation to describe this resistance is based on the following assumptions:

(1) Delamination occurs when the interlaminar shear strength has been exceeded.

(2) Several interply layers could delaminate simultaneously. The detailed deriva-

17

tions are given in the appendix. The resulting equation for the IED from delamination is given by

$$IED = \frac{1}{2} N_{LD} \left(\frac{\beta_{12}\epsilon_{mpS}}{\beta_v \varphi_{\mu 12}} \right)^2 G_{\ell 12} \tag{10}$$

where N_{LD} is the number of delaminated interply layers.

Note that equation (10) is identical with equation (7) except for the coefficient N_{LD}. Therefore, the discussion following equation (7) and the important points noted there apply to equation (10) as well. The additional point to be noted from equation (10) is, that for improved impact resistance, design the part to assure multi-interply delamination. This should be applicable to high velocity impact as well as low.

Longitudinal Impact with Cleavage and Fiber Pullout

This type of impact resistance results in fractured surfaces consisting of broken fibers with debonding and fiber pullout. It was referred to as cleavage with debonding. The governing equation is a combination of equations (3) and (9). The result for the impact energy density for this case is given by

$$IED = (1 - k_v) \frac{S_{fT}^2}{2E_f} \left[\beta_{fT}^2 k_f + \frac{d_f k_{fD}}{4L_c} \left(\frac{\beta_v \varphi_{\mu 12}}{\beta_{12} S^\epsilon_{mpS}} \right) \frac{E_f}{G_{\ell 12}} \right] \tag{11}$$

where L_c is the length of the component subjected to uniform stress which causes fiber fracture.

It is important to note that the fiber pullout contribution (second term in eq. (11)) to impact resistance in equation (11) is strongly dependent on L_c. The following example will illustrate the point. Using typical values for a Modmor-I fiber/matrix composite and assuming 40 percent fiber pullout result in a contribution of approximately $0.3/L_c$. This contribution is negligible for longitudinal impact where L_c is quite large. However, the fiber pullout contribution will be significant in the case of localized or bending impact.

18

The fiber pullout contribution will, in general, be negligible (less than about 1 to 2 percent) if

$$\left(\frac{d_f}{L_c}\right)\left(\frac{E_f}{G_{\ell 12}}\right) < 10^{-5} \tag{12}$$

Equation (11) indicates that composites with high fiber modulus and low intralaminar shear strength are good candidates for high impact resistance. Since equation (11) is a combination of equations (3) and (9), the discussion following these equations applies to equation (11) as well.

HYBRID COMPOSITES TAILOR-MADE FOR IMPROVED IMPACT RESISTANCE

Hybrid composite is the term used for a composite which consists of two or more different fiber/matrix combinations. Typical examples are Modmor-I/epoxy-glass/ epoxy-Modmor-I/epoxy, HTS/epoxy-Thornel-50/epoxy-HTS/epoxy, and others.

Using these composites for improved impact resistance is a major contribution of this investigation. The concept was discovered during the experimental portion of the investigation. It was observed that some of the impacted cantilever specimens (fig. 2(b) longitudinal) exhibited combined fracture modes consisting of fiber breakage, fiber pullout, and interply delamination.

The hybrid composite takes advantage of two or more of these modes to improve impact resistance. It is an important and useful concept in designing structural components in general. The impact resistance of hybrid composites is thus not a material characteristic.

The concept is illustrated here, by applying it to the cantilever structure shown in figure 8. The governing equation for impact energy density is given by

$$\text{IED} = \frac{1}{2}\frac{S^s_{\ell 11T}}{E^s_{\ell 11}}\left\{\left[\frac{1}{9} + \frac{1}{30}\left(\frac{h}{\ell}\right)^2\left(\frac{E^a_{\ell 11}}{G^a_{\ell 12}}\right)\right] + \frac{1}{16N_{LD}}\left(\frac{h}{\ell}\right)\frac{E^s_{\ell 11}}{S^c_{\ell 12}} + \frac{\pi}{16}\left(\frac{N_{fD}d^3_f}{bh\ell}\right)\left(\frac{E^s_{\ell 11}}{S^s_{\ell 12}}\right)\left(\frac{S^s_{fT}}{S^s_{\ell 11T}}\right)^2\right\} \tag{13}$$

where the superscripts a, s, and c represent averaged core-shell, shell, and core, respectively; the subscript 1 refers to unidirectional composite properties along the direction indicated by the numerical subscripts following ℓ; the variables b, h, and ℓ represent width, depth, and length of the cantilever, respectively (see fig. 8 also); d_f is the fiber diameter, N_{fD} is the number of fibers that pulled out, and N_{LD} is the number of layers that delaminated.
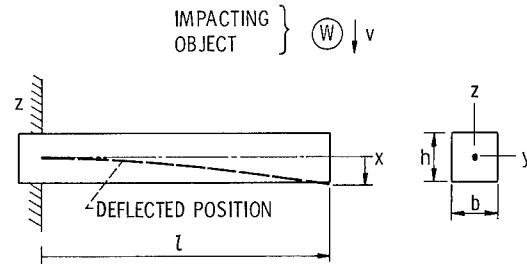
Figure 8. - Cantilever subjected to impact.

Examining equation (13) reveals that the shear contribution depends on $E^a_{\ell 11}/G^a_{\ell 12}$ and that both fiber pullout and delamination depend on the parameter $E^s_{\ell 11}/G^c_{\ell 12}$. This means that, in order to take advantage of the high shear contribution of fiber pullout and/or delamination, high longitudinal modulus, low shear modulus, and low intralaminar strength composites should be selected. Some composites which meet this criterion are Thornel-50, Modmor-I, and PRD-49 fibers in a resin matrix.

There are three other sets of parameters in equation (13) which need careful examination in designing hybrid composites for improved impact resistance. These are (1) $(h/\ell)^2$ for the shear contribution, (2) $h/N_{LD}\ell$ for delamination, and (3) $d^3_f N_{fD}/bh\ell$ for fiber pullout.

The shear contribution will be greater than 3 percent when

$$\left(\frac{\ell}{h}\right)^2 > 10 \, \frac{E^a_{\ell 11}}{G^a_{\ell 12}} \tag{A32}$$

The contribution of the fiber pullout will be greater than 3 percent when

$$\frac{d^3_f N_{fD}}{bh\ell} > 0.02 \, \frac{S^s_{\ell 12S}}{E^s_{\ell 11}} \tag{14}$$

The contribution of the delamination will be greater than 3 percent when

$$\left(\frac{h}{N_{LD}\ell}\right) > 0.06 \left(\frac{S^c_{\ell 12S}}{E^s_{\ell 11}}\right) \tag{15}$$

20

The following expression must be satisfied for delamination:

$$S^c_{\ell 12S} \le \frac{1}{4}\left(\frac{h}{\ell}\right) \min\left(S^s_{\ell 11T}, S^s_{\ell 11c}\right) \tag{16}$$

where the variable $S^s_{\ell 11C}$ denotes longitudinal compressive strength.

Equation (13) in conjunction with the inequalities (eqs. (14) to (16) and (A32)) provides relations which can be used to select parameters in designing composites with improved impact resistance. These equations were used in this investigation to guide the selection of the hybrid composites.

The inequalities (eqs. (A32) and (14) to (16)) can be expressed in terms of constituent properties by using the micromechanics relations for $S_{\ell 11T}$, $S_{\ell 11c}$, $S_{\ell 12S}$, and $E_{\ell 11}$.

APPROXIMATE DESIGN FOR IMPACT

Structural components subjected to impact are designed using an equivalent static load. This type of design is the strength of materials approach and is a first-order approximation (ref. 16, ch. 5).

The governing equations are

$$S^*_\ell = \frac{1}{IF}\, S_\ell \tag{17}$$

where

$$IF = 1 + \left[1 + \frac{2K}{W}\left(H + \frac{v^2}{2g}\right)^{1/2}\right]^{1/2} \tag{18}$$

and where S^*_ℓ is the allowable stress to account for impact, IF is the impact factor, S_ℓ is the static composite strength, K is the spring constant which depends on the type of impact (Relations for K for the types of impact described previously are given in table VI.), W is the impacting weight, H is the height from which W is dropped, and $v^2/2g$ is the potential energy of W.

Note the subscripts in S_ℓ and S^*_ℓ depend on the type of impact loading. For longitudinal impact, for example, the subscripts will be 11T ($S_{\ell 11T}$ and $S^*_{\ell 11T}$). The corresponding spring constant is given in the first line of table VI.

TABLE VI. - SPRING CONSTANTS RELATIONS FOR

VARIOUS IMPACT LOADINGS

Type of impact loading	Spring constant, K
Longitudinal	$E_{l11}\left(\dfrac{A}{l}\right)$
Transverse	$E_{l22}\left(\dfrac{A}{l}\right)$
Shear	$G_{l12}\left(\dfrac{A}{l}\right)$
Cantilever longitudinal (rectangular section including shear contributions)	$\dfrac{E_{l11}bh^3}{4l^3\left[1+1.2\left(\dfrac{h}{l}\right)^2\left(\dfrac{E_{l11}}{G_{l12}}\right)\right]}$
Cantilever transverse (rectangular section including shear contributions)	$\dfrac{E_{l22}bh^3}{4l^3\left[1+1.2\left(\dfrac{h}{l}\right)^2\left(\dfrac{E_{l22}}{G_{l23}}\right)\right]}$

The moduli appearing in the spring constant relations in table VI can be evaluated using micromechanics. Values of these moduli as functions of void and fiber volume ratios are given in reference 7 for several composites. The computer code described in reference 17 may be used to generate additional ones.

EXPERIMENTAL INVESTIGATION

This portion of the investigation consisted of carrying out miniature Izod (ref. 18) impact tests to verify qualitatively the theoretical considerations and concepts described in the THEORETICAL INVESTIGATION.

Materials and Specimen Fabrication

Graphite, glass, and PRD-49 fibers in an epoxy resin matrix were used in the experimental investigation. The various fibers are listed in table VII. All fiber material was drum wound and impregnated with the epoxy resin ERL 2256-ZZL0820 (27.0 pph resin).

TABLE VII. - MINIATURE IZOD IMPACT DATA FOR FIBER/EPOXY[a] COMPOSITES

Fiber	Type	Surface treatment	Fiber volume ratio	Average impact energy				Rank			
				Longitudinal		Transverse		Longitudinal		Transverse	
				cm-N	in. -lb	cm-N	in. -lb	Measured	Predicted	Measured	Predicted
Graphite	Thornel-50S	(b)	0.532	85.9	7.6	7.9	0.7	5	5	3	3
	Thornel-50	Polyvinyl alcohol	.583	208.0	18.4	3.4	.3	4	4	5	5
	HTS	(c)	.523	56.5	5.0	14.7	1.3	6	6	2	2
	Modmor-I	None	.542	215.0	19.0	4.5	.4	3	3	4	4
Glass	S	(d)	0.486	757.0	67.0	15.8	1.4	1	1	1	1
PRD-49	----------	---	-----	280.0	24.8	3.4	0.3	2	2	5	---
Graphite	HTS/Thornel-50S	---	0.598	116.3	10.3	11.3	1.0	3	---	---	---
	HMS/Modmor-I	---	.536	132.0	11.7	----	---	2	---	---	---
	HMS	---	-----	232.0	20.5	----	---	1	---	---	---

[a] Epoxy resin: ERL 2256-ZZL0820 (Union Carbide Corp.); "B" stage of impregnated fiber: 45 min at 93° C, Mylar cover; cure cycle under 35-N/cm^2 (50-psi) pressure: 2 hr at 82° C, 3 hr at 148° C.
[b] Epoxy compatible (Union Carbide Corp.).
[c] Proprietary (Hercules Corp.).
[d] 901 - Owens Corning Fiberglass Co.

Composites were fabricated by means of a unidirectional layup of a number of B-staged plies to yield the thickness desired. Most of the composites consisted of fibers of one particular type. Some hybrid composites were also fabricated that consisted of two fiber types in the layup with selected thickness and position of each. The composites were cured under heat and pressure in a matched-die mold. Complete curing conditions are included in table VII.

Miniature Izod specimens were machined from the fabricated composites in both the longitudinal and transverse directions. The finished specimen dimensions were 7.9 by 7.9 by 37.6 millimeters.

Test Apparatus and Procedure

The impact machine used was a modified Bell Telephone Laboratory pendulum type (fig. 9). The design capacity of the pendulum was 240 centimeter-newtons (27 in. -lb). Addition of weights to the pendulum increased the capacity to 1010 centimeter-newtons (114 in. -lb). The striking velocity of the pendulum was 345 centimeters per second. The Izod specimens were struck at their free end, 22 millimeters from the edge of the
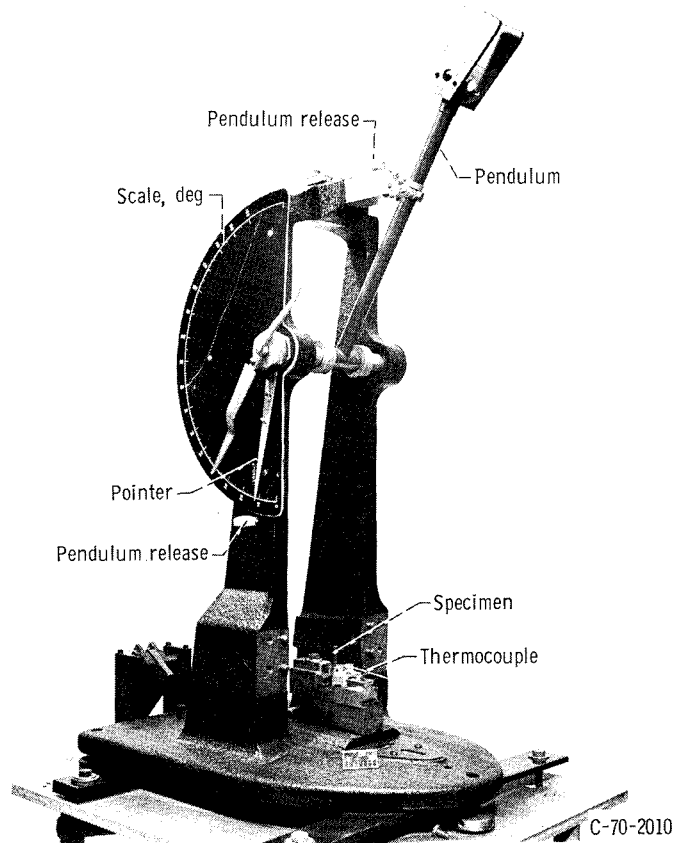
Pendulum release

Pendulum

Scale, deg

Pointer

Pendulum release

Specimen

Thermocouple

C-70-2010

Figure 9. – Miniature Izod pendulum-shaped testing machine.

grip. The specimen length in the grip was 14 millimeters. A "dead weight" load was applied to the grip to assure uniform gripping of specimens.

Composites of one particular fiber were tested in both the longitudinal and transverse directions. Hybrid composites were generally tested in the longitudinal direction with the plies parallel to the striking pendulum. The angular displacement of the pendulum after impact was an inverse measure of the impact energy. Typical fractured specimens from this method of testing are shown in figure 10.

24

Thornel-50S Thornel-50 HTS Modmor-I S-glass PRD-49

Longitudinal

Transverse

HTS/Thornel-50S   HMS/Modor-I   HMS/PRD-49

Hybrid composites   C-71-746
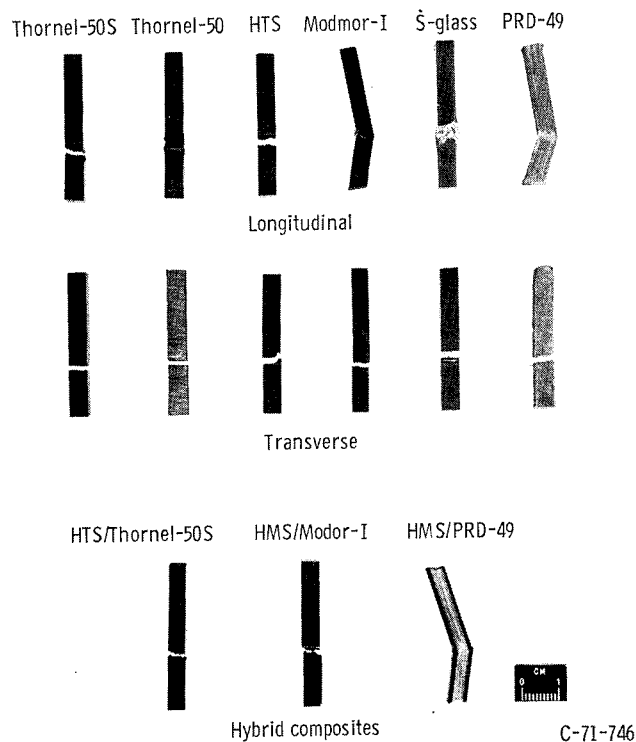
Figure 10. – Miniature Izod impact specimens showing various modes of failure.

EXPERIMENTAL RESULTS AND DISCUSSION

Longitudinal and Transverse Impact

Several specimens of each composite system were tested in longitudinal and transverse impact; also specimens from the matrix system were tested. The results are presented in figure 11. The scatter is indicated by the light lines within the bar.

Photomicrographs of typical fracture surfaces are shown in figure 12. Note the fracture modes, cleavage, and cleavage with fiber pullout. (Photographs of the fractured specimens are shown in fig. 10.) The observed fracture modes for various composites are summarized in table VIII. Impact resistance is plotted against short-beam intralaminar shear strengths for several of these composites in figure 13. The intralaminar shear strengths are needed to assist with the theoretical impact resistance ranking of the test specimens.

Measured results of longitudinal impact normal and parallel to the lamination directions were identical. This is to be expected in unidirectional composites with nonmetallic matrices.
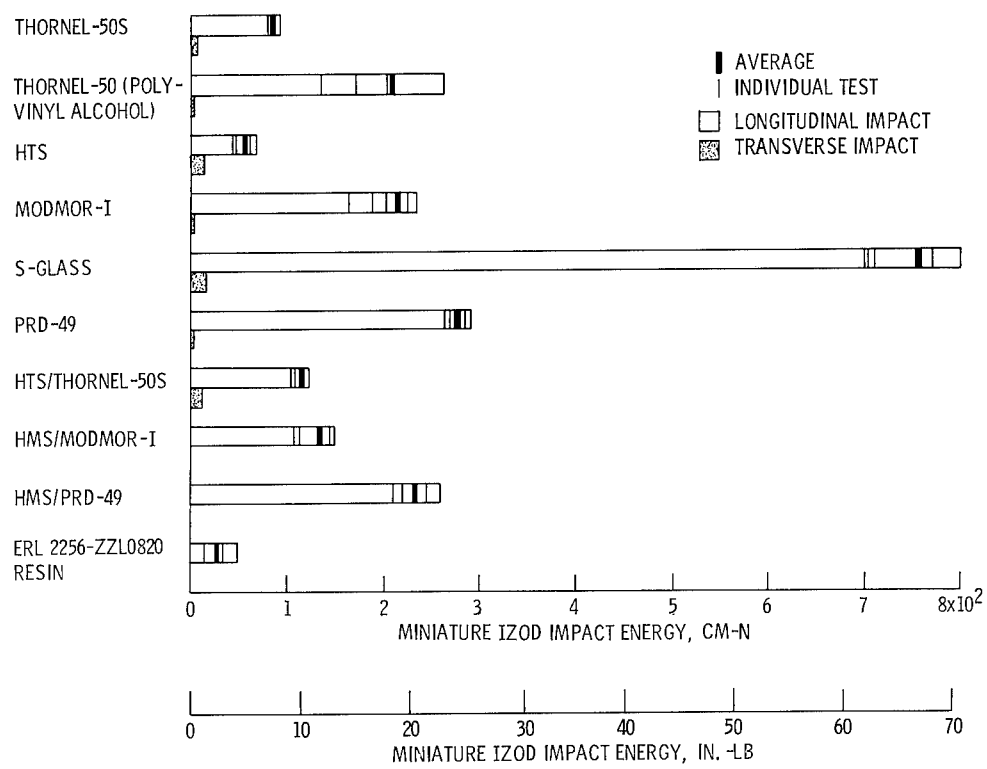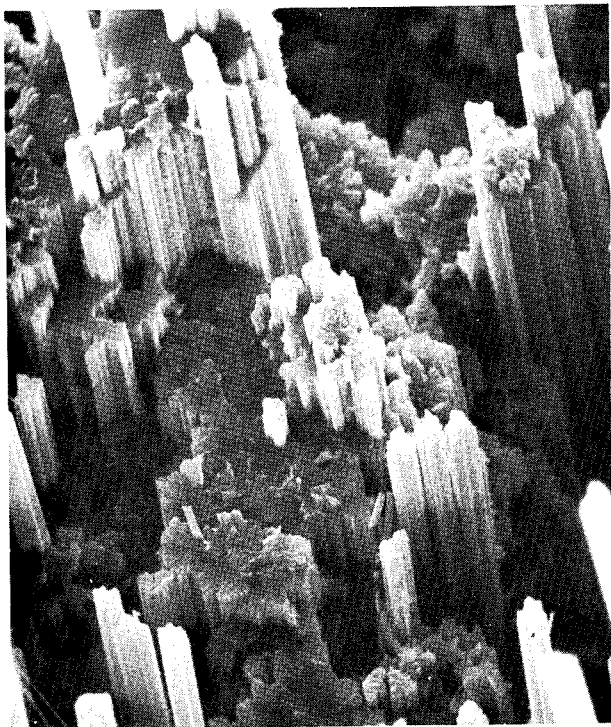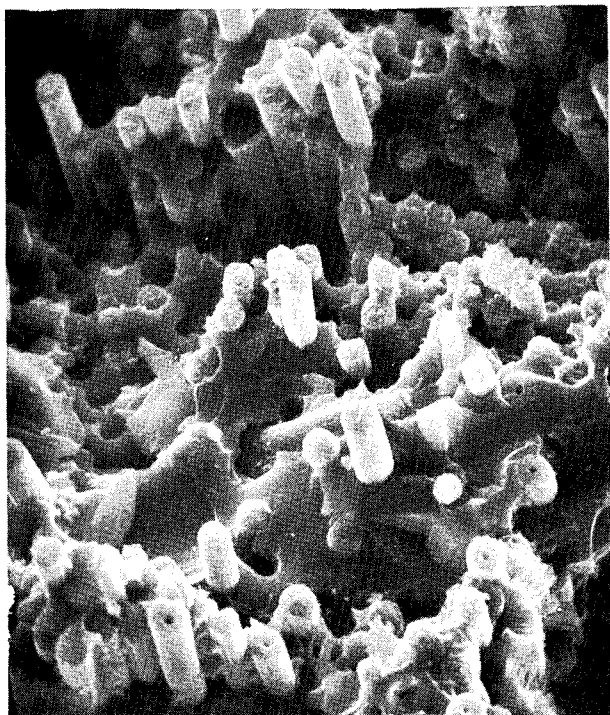
25

Figure 11. - Miniature Izod impact energy of fiber/ERL 2256-ZZL0820 composites.
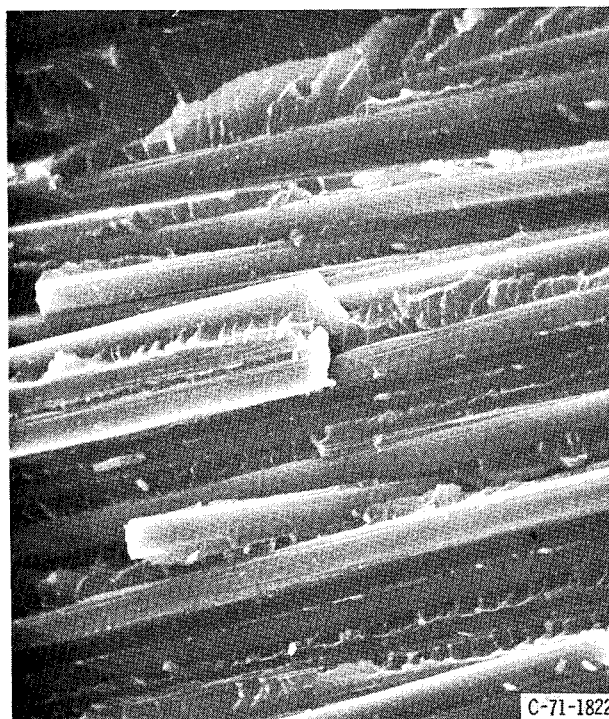
(a) Longitudinal fracture of Thornel-50S composite.

(b) Transverse fracture of Thornel-50S composite.

(c) Longitudinal fracture of HTS composite.

(d) Transverse fracture of HTS composite.

C-71-1822

Figure 12. - Scanning electron micrographs of fracture surfaces of graphite composites resulting from impact load. X600.

TABLE VIII. - SUMMARY OF OBSERVED FRACTURE MODES ON

MINIATURE IZOD IMPACT TEST SPECIMENS

| Fiber/epoxy composites	Longitudinal			Transverse	
	Brittleness	Debonding plus fiber pullout	Delamination	Brittleness	Fiber splitting
HTS	Yes	Little	---	Yes	---
Thornel-50S	Yes	Some	---	Yes	Yes
Thornel-50 (polyvinyl alcohol)	---	Yes	Yes	Yes	Yes
Modmor-I	---	Yes	Yes	Yes	---
S-glass	Yes	Very little	One layer	Yes	---
PRD-49	---	---	---	---	---
HTS/Thornel-50S/HTS	Yes	Yes	Yes	Yes	---
HMS/Modmor-I/HMS	Yes	Yes	Yes	---	---
HMS/PRD-49/HMS	Yes	Yes	Yes	Yes	---
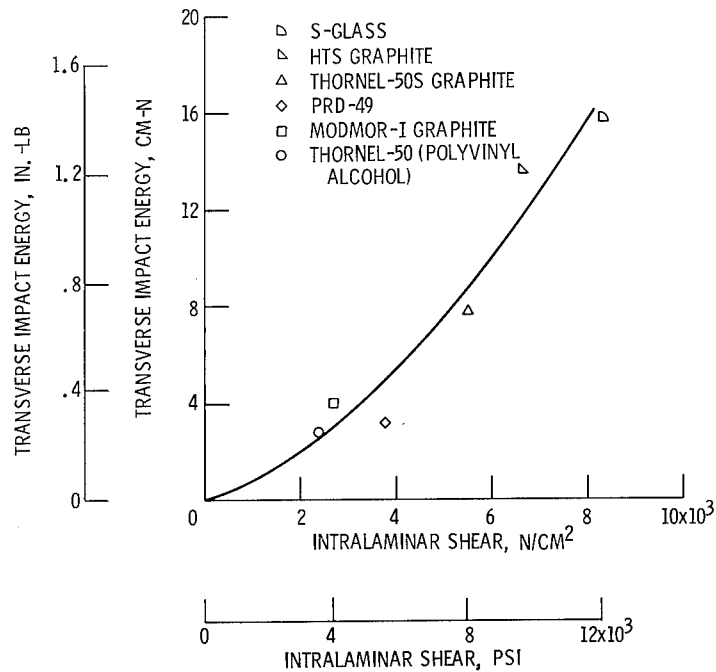
Figure 13. - Experimental results of transverse impact energy as a function of intralaminar shear for various fiber/resin composites.

Discussion of Experimental Results and Comparison of Ranking

Examination of table VIII and figure 11 reveal the following:

(1) Those composites which exhibit more than one fracture mode have higher impact resistance in general.

(2) Composite transverse impact results in brittle fracture and the value is considerably lower than that of the matrix. Some fiber splitting occurs in the Thornel-fiber composites.

(3) The hybrid composite experienced two or more fracture modes.

Averaged values of the experimental results are summarized in table VII. The last four columns of this table contain the ranking with respect to impact resistance. As can be seen, the measured and predicted ranking is identical. The predicted ranking was obtained as follows: For the longitudinal ranking, equation (13) was used in conjunction with table I and figure 13. For the transverse ranking equation (6) was used in conjunction with figure 13. The use of figure 13 for the transverse strength is acceptable because both intralaminar shear and transverse composite strengths exhibit similar trends.

It is interesting to note in table VI that one of the hybrid composites had larger impact resistance than either of the two constituent composites. The explanation is that the hybrid composite had more delaminated surfaces. This, of course, is the essence of the hybrid composite concept for improved impact resistance.

The important point to keep in mind from this discussion is that theoretical expressions can be constructed to predict impact resistance at least on a qualitative basis. These expressions can be used to guide research for constituent materials and design concepts for improved impact resistance.

CONCLUSIONS

Results from this investigation of gross-type-impacts of composites involving relatively long impact contact times lead to the following conclusions:

1. The impact resistance of unidirectional composites is ranked using elementary composite mechanics, and criteria are presented to guide design for improved resistance.

2. Theoretical results show that, in composites with high fiber-to-matrix modulus ratios, the longitudinal impact resistance is fiber controlled. When this ratio is twenty, the matrix contribution is less than 5 percent. However, the transverse and shear impact resistances are matrix controlled.

3. Theoretical results show that, in composites with fiber-to-matrix modulus or strength ratios of about four, the longitudinal impact resistance could be matrix controlled. In this case, the presence of microresidual stresses decreases the impact resistance considerably.

4. Theoretical considerations indicate that the impact resistance can be improved by designing the composite so that fiber breakage, fiber debonding with fiber pullout, and partial delamination take place at the same time. Any combinations of these fracture modes will also improve the impact resistance.

5. Theoretical considerations also show that the impact resistance is sensitive to void and fiber contents and to certain fabrication factors which are reflected in the in-situ constituent properties.

6. The experimental results indicate three prevalent longitudinal failure modes due to impact. These are cleavage, cleavage with some fiber pullout, and cleavage combined with partial delamination due to intralaminar shear failure.

7. The transverse failure mode was cleavage. The fracture surface included matrix fracture, fiber debonding, and some fiber splitting. The experimental results showed that the impact resistance was the same whether the specimen was impacted parallel or normal to the lamination direction.

8. Ranking of predicted results was in good agreement with that of measured results from notched Charpy impact, cryogenic fracture toughness, stress intensity, and unnotched Izod impact.

9. The hybrid composite concept is an efficient composite design to combine high strength and high stiffness with high impact resistance.

Lewis Research Center,
    National Aeronautics and Space Administration,
        Cleveland, Ohio, May 18, 1971,
            129-03.

APPENDIX – DETAILED DERIVATIONS OF GOVERNING EQUATIONS

The detailed derivations which lead to the equations presented and discussed in the section THEORETICAL INVESTIGATION are as follows:

Longitudinal impact (see fig. 1(a)):

$$U_L = \frac{1}{2} S_{\ell 11T} \epsilon^*_{\ell 11T} V = \frac{S^2_{\ell 11T}}{2E_{\ell 11}} V \tag{A1}$$

From micromechanics (refs. 7 and 8)

$$E_{\ell 11} = (1 - k_v)E_f \left[k_f + (1 - k_f) \frac{E_m}{E_f} \right] \tag{A2}$$

$$S_{\ell 11T} = (1 - k_v)S_{fT} \left[k_f \beta_{fT} + \beta_m (0 - k_f) \frac{E_m}{E_f} \right] \tag{A3}$$

Substituting equations (A2) and (A3) in equation (A1), neglecting terms E_m/E_f, and simplifying yield

$$IED = \frac{U_L}{V} = \frac{(1 - k_v)k_f \beta^2_{fT} S^2_{fT}}{2E_f} \tag{A4}$$

Transverse impact (see fig. 1(b)):

$$U_T = \frac{1}{2} S_{\ell 22T} \epsilon^*_{\ell 22T} V = \frac{S^2_{\ell 22T}}{2E_{\ell 22}} V \tag{A5}$$

From micromechanics (ref. 8)

$$S_{\ell 22T} = \beta_{22T} \frac{\epsilon_{mpT}}{\beta_v \varphi_{\mu 22}} E_{\ell 22} \tag{A6}$$

Using equation (A6) in equation (A5) and simplifying result in

$$\text{IED} = \frac{U_T}{V} = \frac{1}{2}\left(\frac{\beta_{22T}\epsilon_{mpT}}{\beta_v{}^\varphi \mu_{22}}\right)^2 E_{l\,22} \tag{A7}$$

Shear impact (see fig. 1(c)):

$$U_S = \frac{1}{2} S_{l\,12S}\epsilon^*_{l\,12S}V = \frac{S^2_{l\,12S}}{2G_{l\,12}}V \tag{A8}$$

From micromechanics (ref. 8)

$$S_{l\,12S} = \beta_{12S}\frac{\epsilon_{mpS}}{\beta_v{}^\varphi \mu_{12}}G_{l\,12} \tag{A9}$$

Using equation (A9) in equation (A8) and simplifying yield

$$\text{IED} = \frac{U_S}{V} = \frac{1}{2}\left(\frac{\beta_{12S}\epsilon_{mpS}}{\beta_v{}^\varphi \mu_{12}}\right)^2 G_{l\,12} \tag{A10}$$

Debonding Contribution

The work done to pull out N_{fD} broken fibers a distance l_{cr} is given by (refs. 3 and 4)

$$U_{FPO} = N_{fD}\int_0^{l_{cr}} x\tau_{xy}\pi d_f\,dx \tag{A11}$$

$$U_{FPO} = \frac{1}{2}N_{fD}\pi d_f\tau_{xy}l_{cr}^2 \tag{A12}$$

From force equilibrium and assuming uniform shear, we get

$$\ell_{cr}\tau_{xy}\pi d_f = \frac{1}{4}\pi d_f^2 S_{fT}$$

$$\ell_{cr} = \frac{1}{4}d_f\frac{S_{fT}}{\tau_{xy}} \tag{A13}$$

Using equation (A13) in equation (A12) and simplifying yield

$$U_{FPO} = \frac{N_{fD}\pi d_f^3}{32}\frac{S_{fT}^2}{\tau_{xy}} \tag{A14}$$

where τ_{xy} is the shear interface bond strength. It is generally accepted in the composites community that $S_{\ell 12S}$ is a measure of interface bond strength. Letting $\tau_{xy} = S_{\ell 12S}$ in equation (A14) results in

$$U_{FPO} = N_{fD}\pi d_f^3 \frac{S_{fT}^2}{32S_{\ell 12S}} \tag{A15}$$

Multiply and divide equation (A15) by the area of the fractured surface as follows:

$$U_{FPO} = \frac{N_{fD}\pi d_f^3}{A}\frac{S_{fT}^2 A}{32S_{\ell 12S}} \tag{A16}$$

By definition

$$\frac{N_{fD}\pi d_f^2}{4A} = (1 - k_v)k_f \tag{A17}$$

Using equation (A17) in equation (A16) and dividing through by the area give

$$IED = \frac{U_{FPO}}{Ad_f} = (1 - k_v)k_f\frac{S_{fT}^2}{8S_{\ell 12S}} \tag{A18}$$

Using the definition for $S_{l\,12S}$ from equation (A7) in equation (A18) results in the desired result

$$IED = \frac{1}{8}(1 - k_v)k_f\left(\frac{\beta_v{}^\varphi \mu 12}{\beta_{12S}{}^\epsilon mpS}\frac{S_{fT}^2}{G_{l\,12}}\right) \qquad (A19)$$

Delamination Contribution

The energy expanded in delaminating several interply layers of area A_D over a length l_D is given by

$$U_D = \frac{1}{2}\sum_{i=1}^{N_{LD}}\left(\frac{S_{l\,12S}^2}{G_{l\,12}}\right)_i (A_D l_D)_i \qquad (A20)$$

Assuming the sum in equation (A20) is independent of i yields

$$U_D = \frac{1}{2}(N_{LD}A_D l_D)\frac{S_{l\,12S}^2}{G_{l\,12}} \qquad (A21)$$

and the impact energy density is

$$IED = \frac{U_D}{A_D l_D} = N_{LD}\frac{S_{l\,12S}^2}{2G_{l\,12}} \qquad (A22)$$

Using equation (A9) for $S_{l\,12S}$ in equation (A22) and simplifying results in

$$IED = \frac{1}{2}N_{LD}\left(\frac{\beta_{12S}{}^\epsilon mpS}{\beta_v{}^\varphi \mu 12}\right)^2 G_{l\,12} \qquad (A23)$$

Combined Longitudinal and Fiber Pullout

The energy expended to produce this combination of modes is a combination of equations (A4) and (A16) each multiplied by the appropriate volume; that is,

$$U = \left[\frac{(1 - k_v)k_f\beta_{fT}^2 S_{fT}^2}{2E_f} L_c A + \frac{1}{8}(1 - k_v)k_{fD}d_f A \left(\frac{\beta_v \pi \varphi \mu 12}{\beta 12 S^\epsilon mpS}\right)\frac{S_{fT}^2}{G_{l\,12}} \right] \tag{A24}$$

Factoring out $(1 - k_v)L_c A \left(S_{fT}^2/2E_f\right)$ and dividing both sides by $L_c A$ yield

$$IED = \frac{U}{L_c A} = \frac{1}{2}(1 - k_v)\frac{S_{fT}^2}{E_f}\left[k_f\beta_{fT}^2 + \frac{1}{4}k_{fD}\left(\frac{d_f}{L_c}\right)\left(\frac{\beta_v \varphi \mu 12}{\beta 12 S^\epsilon mpS}\right)\frac{E_f}{G_{l\,12}}\right] \tag{A25}$$

Note that in equation (A25) k_f refers to the fiber volume ratio for the whole cross section, while k_{fD} refers to the volume ratio of the pullout fibers.

Combined Longitudinal Fiber Pullout and Delamination for a

Rectangular Cantilever (See fig. 8)

The energy expended in delaminating several layers simultaneously for a cantilever is given by

$$U = \frac{1}{2} N_{LD}b l_D^2 S_{l\,12S} \tag{A26}$$

Assuming simultaneous tensile failure and delamination near the neutral plane of the cantilever yields

$$N_{LD}S_{l\,12S}l_D b = \frac{1}{4}hbS_{l\,11T}$$

and

$$\ell_D = \frac{bS_{\ell 11T}}{4N_{LD}S_{\ell 12S}} \tag{A27}$$

Using equation (A27) in equation (A26) and simplifying yield

$$U = \frac{bh^2}{32N_{LD}} \frac{S^2_{\ell 11T}}{S_{\ell 12S}} \tag{A28}$$

the total energy expended to fracture the cantilever in combined modes is given by

$$U = U_{FLEXURAL} + U_{SHEAR} + U_{FIBER\ PULLOUT} + U_{DELAMINATION} \tag{A29}$$

The flexural and shear energies are given by

$$U_{FLEXURAL} + U_{SHEAR} = \int_0^\ell \int_{-b/2}^{h/2} \frac{1}{2}\left[\left(\frac{\sigma_x^2}{E_x}\right) + \left(\frac{\sigma_{xy}^2}{G_{xy}}\right)\right] b\ dz\ dx \tag{A30}$$

Carrying out the integration in equation (A30), requiring that the cantilever will fail first by tension, and simplifying result in

$$U_{FLEXURAL} + U_{SHEAR} = \frac{1}{2}(bh\ell)\frac{S^2_{\ell 11T}}{E_{\ell 11}}\left[\frac{1}{9} + \frac{1}{30}\left(\frac{b}{\ell}\right)^2 \frac{E_{\ell 11}}{G_{\ell 12}}\right] \tag{A31}$$

The shear contribution (second term in eq. (A31)) will be less than 3 percent if

$$\left(\frac{\ell}{h}\right)^2 > 10\ \frac{E_{\ell 11}}{G_{\ell 12}} \tag{A32}$$

For a hybrid composite where the shell and core are made from different composites, equation (A31) is approximated by

36

$$U_{\text{FLEXURAL}} + U_{\text{SHEAR}} = \frac{1}{2}\,(bh\ell)\,\frac{\left(S^2_{\ell\,11T}\right)^2}{E^s_{\ell\,11}}\left[\frac{1}{9} + \frac{1}{30}\left(\frac{h}{\ell}\right)^2\frac{E^a_{\ell\,11}}{G^a_{\ell\,12}}\right] \tag{A33}$$

where

$$E^a_{\ell\,11} = k_s E^s_{\ell\,11} + k_c E^c_{\ell\,11} \tag{A34}$$

and

$$G^a_{\ell\,12} = G^s_{\ell\,12}\ \frac{1}{k_s + k_c\,\dfrac{G^s_{\ell\,12}}{G^c_{\ell\,12}}} \tag{A35}$$

The notation in equations (A33) to (A35) is as follows: superscript a refers to averaged properties; k is a ratio; superscripts and subscripts s and c refer to shell and core, respectively.

The fiber pullout energy is given by equation (A15). Using equations (A33), (A15), and (A28) in equation (A29), simplifying, and rearranging result in

$$\text{IED} = \frac{U}{bh\ell} = \frac{1}{2}\frac{S^2_{\ell\,11T}}{E_{\ell\,11}}\left\{\left[\frac{1}{9} + \frac{1}{30}\left(\frac{h}{\ell}\right)^2\left(\frac{E^a_{\ell\,11}}{G^a_{\ell\,12}}\right)\right] + \frac{1}{16N_{LD}}\left(\frac{h}{\ell}\right)\left(\frac{E^s_{\ell\,11}}{S^c_{\ell\,12S}}\right)\right.$$
$$\left. + \frac{\pi}{16}\left(\frac{N_{fD}d^3_f}{bh\ell}\right)\left(\frac{E^s_{\ell\,11}}{S^s_{\ell\,12}}\right)\left(\frac{S^s_{ft}}{S^s_{\ell\,11T}}\right)^2\right\} \tag{A36}$$

subject to

$$S_{\ell\,12S} \approx \frac{1}{4}\left(\frac{h}{\ell}\right)\min(S_{\ell\,11T},\, S_{\ell\,11C}) \tag{A37}$$

Equation (A37) supplies the condition to satisfy the assumption of either simultaneous tensile failure or simultaneous compressive failure and delamination. Equation (A33) can be expressed in terms of constituent material variables by using the micromechanics definitions for strengths and moduli.

Longitudinal Impact Resistance When Matrix Is Controlling and Effects of Microresidual Stresses

This case arises when $E_f/E_m < 10$. Fiber/metallic matrix composites usually meet this requirement. The energy stored in the composite is given by (refer to fig. 1(a))

$$U = \frac{1}{2} S_{\ell 11T} \epsilon^*_{\ell 11} V = \frac{S^2_{\ell 11T}}{2E_{\ell 11}} V \tag{A38}$$

The micromechanics equation for $S_{\ell 11T}$ when the matrix controls the failure is given by

$$S_{\ell 11T} = (1 - k_v) S_{mT} \left[(1 - k_f)\beta_m + k_f \frac{E_f}{E_m} \right] \tag{A39}$$

Using equation (A39) in equation (A38) and simplifying yield

$$IED = \frac{U}{V} = \frac{E_{\ell 11} S^2_{mT}}{2E^2_m} \tag{A40}$$

The presence of microresidual stresses will affect S_{mT}. This effect will equal the magnitude of the residual stress. The available matrix strength for resisting impact is

$$S^*_{mT} = S_{mT} - \sigma_{mR} \tag{A41}$$

where σ_{mR} is the microresidual stress in the matrix. Using strength of materials methods, it can be shown that

38

$$\sigma_{mR} = \frac{k_f \, \Delta T(\alpha_f - \alpha_m) E_f E_m}{E_{\ell\,11}} \tag{A42}$$

Substituting S_{mT}^* for S_{mT} in equation (A40) and using equation (A42) result in

$$\left. \begin{aligned} IED &= aE_{\ell\,11}\left(S_{mT} - B\,\frac{k_f}{E_{\ell\,11}}\right)^2 \\[2mm] a &= \frac{1}{2E_m^2} \\[2mm] B &= \Delta T(\alpha_f - \alpha_m) E_f E_m \end{aligned} \right\} \tag{A43}$$

Corresponding equations for the fiber are obtained in a similar manner. The result will be analogous to equation (A43) with subscripts f and m interchanged.

REFERENCES

1. Tetelman, A. S.: Fracture Processes in Fiber Composite Materials. Composite Materials: Testing and Design. Spec. Tech. Publ. 460, ASTM, 1969, pp. 473-502.

2. Novak, R. C.: Fracture in Graphite Filament Reinforced Epoxy Loaded in Shear. Composite Materials: Testing and Design. Spec. Tech. Publ. 460, ASTM, 1969, pp. 540-549.

3. Kelly, A.: Interface Effects and the Work of Fracture of a Fibrous Composite. Rep. NPL-IMS-10, National Physical Lab., England, Feb. 1970.

4. Outwater, J. O.; and Murphy, M. C.: Fracture Energy of Unidirectional Laminates. Modern Plastics, vol. 47, no. 9, Sept. 1970, p. 160.

5. Rotem, A.; and Lifshitz, J. M.: Longitudinal Strength of Unidirectional Fibrous Composite Under High Rate of Loading. Proceedings of the 26th Annual Society of the Plastics Industry Conference, 1971, section 10-G.

6. Chiao, T. T.; and Moore, R. L.: Stress-Rupture of S-Glass/Epoxy Multifilament Strands. J. Composite Mat., vol. 5, Jan. 1971, pp. 2-11.

7. Chamis, Christos C.: Thermoelastic Properties of Unidirectional Filamentary Composites by a Semiemperical Micromechanics Theory. Science of Advanced Materials and Process Engineering Proceedings. Vol. 14. Western Periodicals Co., 1968, Paper I-4-5.

8. Chamis, Christos C.: Failure Criteria for Filamentary Composites. NASA TN D-5367, 1969.

9. Daniel, I. M.: Photoelastic Study of Crack Propagation in Composite Models. J. Composite Mat., vol. 4, no. 2, Apr. 1970, pp. 178-190.

10. Broutman, L. J.; and Sahu, S.: The Effect of Interfacial Bonding on the Toughness of Glass Filled Polymers. Proceedings of the 26th Annual Society of the Plastics Industry Conference, 1971, section 14-C.

11. McGarry, Frederick J.; and Mandell, J. F.: Fracture Toughness of Fiber Reinforced Composites. Res. Rep. R70-79, Massachusetts Inst. Tech., Dec. 1970.

12. Aulenbach, T. H.; Schulz, W. J.; and McGarry, F. J.: Fracture Toughness Testing of Fibrous Glass Resin Composites. Proceedings of the 25th Annual Society of the Plastics Industry Conference, 1970.

13. Bacon, J. F.: Investigation of the Kinetics of Crystalization of Several High Temperature Glass Systems. Rep. J910939-3, United Aircraft Research Lab., Sept. 1970.

14. Cooper, R. E.: The Work-To-Fracture of Brittle-Fibre Ductile-Matrix Composites. J. Mech. Phys. Solids, vol. 8, no. 3, June 1970, pp. 179-187.

15. Corten, H. T.: Influence of Fracture Toughness and Flows on the Interlaminar Shear Strength of Fibrous Composites. Fundamental Aspects of Fiber Reinforced Plastic Composites. R. T. Schwartz and H. S. Schwartz, eds., Interscience Publ., 1968, pp. 89-107.

16. Marin, Joseph: Mechanical Behavior of Engineering Materials. Prentice-Hall, Inc., 1962.

17. Chamis, Christos C.: Computer Code for the Analysis of Multilayered Fiber Composites - Users Manual. NASA TN D-7013, 1971.

18. Compton, William A.; and Steward, Keith P.: Composite Materials for Turbine Compressors Test Specifications Manual. Rep. RDR-1462-6, Solar Div., International Harverter (AFML-TR-68-31, pt. 2, DDC No. AD-840035), Apr. 1968.

19. Simon, Robert A.; and Alfring, Richard: Properties of Graphite Fiber Composites at Cryogenic Temperatures, June 1967 - August 1969. Rep. NOLTR-69-183, Naval Ordnance Lab. (NASA CR-72652), May 13, 1970.

FIRST CLASS MAIL
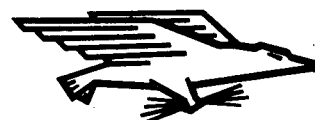
```
012 001 C1 U  32 710813 S00942DS
DEPT OF THE ARMY
PICATINNY ARSENAL
PLASTICS TECHNICAL EVALUATION CENTER
ATTN: SMUPA-VP3
DOVER NJ 07801
```

"The aeronautical and space activities of the United States shall be conducted so as to contribute . . . to the expansion of human knowledge of phenomena in the atmosphere and space. The Administration shall provide for the widest practicable and appropriate dissemination of information concerning its activities and the results thereof."

— NATIONAL AERONAUTICS AND SPACE ACT OF 1958

NASA SCIENTIFIC AND TECHNICAL PUBLICATIONS

TECHNICAL REPORTS: Scientific and technical information considered important, complete, and a lasting contribution to existing knowledge.

TECHNICAL NOTES: Information less broad in scope but nevertheless of importance as a contribution to existing knowledge.

TECHNICAL MEMORANDUMS: Information receiving limited distribution because of preliminary data, security classification, or other reasons.

CONTRACTOR REPORTS: Scientific and technical information generated under a NASA contract or grant and considered an important contribution to existing knowledge.

TECHNICAL TRANSLATIONS: Information published in a foreign language considered to merit NASA distribution in English.

SPECIAL PUBLICATIONS: Information derived from or of value to NASA activities. Publications include conference proceedings, monographs, data compilations, handbooks, sourcebooks, and special bibliographies.

TECHNOLOGY UTILIZATION PUBLICATIONS: Information on technology used by NASA that may be of particular interest in commercial and other non-aerospace applications. Publications include Tech Briefs, Technology Utilization Reports and Technology Surveys.

Details on the availability of these publications may be obtained from:

SCIENTIFIC AND TECHNICAL INFORMATION OFFICE

NATIONAL AERONAUTICS AND SPACE ADMINISTRATION
Washington, D.C. 20546